Hindawi Publishing Corporation
BioMed Research International
Volume 2016, Article ID 8609274, 12 pages
http://dx.doi.org/10.1155/2016/8609274

Research Article

[^{18}F]FDG Uptake in the Aortic Wall Smooth Muscle of Atherosclerotic Plaques in the Simian Atherosclerosis Model

Takayuki Iwaki,[1] Hiroshi Mizuma,[2] Kazuya Hokamura,[1] Hirotaka Onoe,[2] and Kazuo Umemura[1]

[1]*Department of Pharmacology, Hamamatsu University School of Medicine, Hamamatsu, Japan*
[2]*Bio-Function Imaging Team, Imaging Platform and Innovation Group, Division of Bio-Function Dynamics Imaging, RIKEN Center for Life Science Technologies, Kobe, Japan*

Correspondence should be addressed to Takayuki Iwaki; tiwaki@hama-med.ac.jp

Received 18 August 2016; Revised 2 November 2016; Accepted 28 November 2016

Academic Editor: Venkatesh Mani

Atherosclerosis is a self-sustaining inflammatory fibroproliferative disease that progresses in discrete stages and involves a number of cell types and effector molecules. Recently, [^{18}F]fluoro-2-deoxy-D-glucose- ([^{18}F]FDG-) positron emission tomography (PET) has been suggested as a tool to evaluate atherosclerotic plaques by detecting accumulated macrophages associated with inflammation progress. However, at the cellular level, it remains unknown whether only macrophages exhibit high uptake of [^{18}F]FDG. To identify the cellular origin of [^{18}F]FDG uptake in atherosclerotic plaques, we developed a simian atherosclerosis model and performed PET and ex vivo macro- and micro-autoradiography (ARG). Increased [^{18}F]FDG uptake in the aortic wall was observed in high-cholesterol diet-treated monkeys and WHHL rabbits. Macro-ARG of [^{18}F]FDG in aortic sections showed that [^{18}F]FDG was accumulated in the media and intima in the simian model as similar to that in WHHL rabbits. Combined analysis of micro-ARG with immunohistochemistry in the simian atherosclerosis model revealed that most cellular [^{18}F]FDG uptake observed in the media was derived not only from the infiltrated macrophages in atherosclerotic plaques but also from the smooth muscle cells (SMCs) of the aortic wall in atherosclerotic lesions.

1. Introduction

Atherosclerosis is a self-sustaining inflammatory fibroproliferative disease that progresses with a number of cell types and effector molecules in sequential and discrete stages [1]. Lipid metabolism abnormalities, elevated low-density lipoprotein (LDL) and triglyceride levels, and/or reduced high-density lipoprotein (HDL) levels are known to be heavily involved in the genesis and progression of atherosclerosis in humans in which type-IIa hypercholesterolemia is frequently observed, with elevated plasma LDL-cholesterol (LDL-C) due to reduced efficiency or lack of the LDL receptor (LDLr). In animal models, LDLr-deficient mice ($Ldlr^{-/-}$) [2] do not develop spontaneous atherosclerotic plaques with normal chow diet due to the presence of apolipoprotein-B editing catalytic polypeptide-1 (Apobec1) in their liver. However, mice deficient in both LDLr and Apobec1 ($Ldlr^{-/-}$/$Apobec1^{-/-}$) [3] or apoE ($Apoe^{-/-}$) [4] exhibit the formation of spontaneous atherosclerotic plaques with normal chow diet. In addition, Watanabe heritable hyperlipidemic (WHHL) rabbits [5], in which the LDLr is deleted [6], have also been used to assess the initiation and/or progression of atherosclerotic plaques. These small animal models have been frequently used because of advantages such as easy handling, reduced ethical concerns, and well-characterized genetic backgrounds. However, species-related differences between these animals and humans need to be considered before translating primary research data to humans.

Due to the similarities between nonhuman primates and humans in terms of genetics and metabolism, larger animals are considered to be better models for testing possible therapeutic compounds [7] and investigating human atherosclerosis [8]. Noninvasive methods to evaluate atherosclerosis are desired for extrapolating findings obtained in nonhuman primates to humans. Indeed, although various methods, such

as ultrasonography, magnetic resonance imaging (MRI), and X-ray computed tomography (CT) [9–11], have been used to detect plaques, they do not detect pertinent biological activities, namely, metabolic status, severity of inflammation, and fragility of plaques, which are critical determinants of the status of atherosclerotic plaques.

Positron emission tomography (PET) with the tracer [^{18}F]fluoro-2-deoxy-D-glucose ([^{18}F]FDG), a glucose analog, has been reported to be a promising tool for identifying inflammatory loci in various pathophysiologic conditions, including atherosclerotic plaques in mice [12], rabbits [13], and humans [14]. This tracer has been used to detect vulnerable atherosclerotic plaques associated with macrophage infiltration into atherosclerotic lesions. However, it has been claimed that [^{18}F]FDG uptake and macrophage content in peripheral arteries of patients with atherosclerosis are not significantly correlated, indicating that other cell types, such as arterial endothelial and smooth muscle cells, might be contributing to human atherosclerosis imaging [15]. To define the significance of [^{18}F]FDG uptake in atherosclerotic lesion pathology, we developed a simian atherosclerosis model, which is expected to be more similar to the human disease, because of physiological, biochemical, and metabolic similarities of monkeys to humans [16]. For this reason, using this simian model of atherosclerosis, we performed in vivo [^{18}F]FDG-PET to assess disease progression and an ex vivo macro- and micro-autoradiography (ARG) to further identify the localization of [^{18}F]FDG in atherosclerotic plaques in aortas at tissue and cellular levels, respectively.

2. Materials and Methods

2.1. Animals. Seventeen male cynomolgus monkeys *(Macaca fascicularis)* weighing between 3.3 and 6.2 kg were purchased from Japan SLC Inc. (Hamamatsu, Japan). The monkeys were fed once daily with approximately 150 g of high-cholesterol (containing 6% corn oil and 0.5% cholesterol; Oriental Yeast Co., Ltd., Tokyo, Japan) or normal diet. The monkeys were randomized into 5 groups as follows: normal diet and high-cholesterol diet for 7, 12, 18, and 24 months. Two male WHHL rabbits which are developed as a disease model for spontaneous hypercholesterolemia and atherosclerosis and two Japanese white rabbits were purchased from Oriental Yeast Co. Ltd. (Tokyo, Japan). The animals were housed individually in a cage under 12-hour light/dark cycle (light off 8 PM) with freely accessed food and water. All experimental procedures were conducted in accordance with the animal care and use guidelines of the NIH and performed following approval of the study ethics by the Institutional Animal Care and Use Committee of RIKEN Kobe Branch (permit number, MAH20-01) and Hamamatsu University School of Medicine Animal Committee (permit number, 2008048).

2.2. Biochemical Parameters and Histological Analyses

2.2.1. Biological Parameters. For the measurement of biochemical parameters, blood was collected intracardially at the time of euthanasia. The plasma samples were obtained by centrifugation at 1500 ×g for 10 min at 4°C and then were stored at −30°C until the assay. The following biochemical parameters were measured using an automated biochemical analyzer (JCA-BM2250, JEOL Co. Ltd., Tokyo, Japan): total cholesterol (C), HDL-C, free-C, and triglycerides. The LDL-C was also assessed in several of the samples using high performance liquid chromatography (HPLC).

2.2.2. Analysis of Atherosclerotic Lesions in Whole Aorta. Aortas were cut longitudinally, exposing the lumen, and aortic trees were placed on a black plastic plate with the lumen-side up. A plate was then placed over the aortic lumens to hold them in place during fixation. The aortas were fixed in periodate-lysine-paraformaldehyde (PLP) for 16 h at room temperature, rinsed with H_2O, and stained with Sudan IV (Sigma Japan, Tokyo, Japan) solution (Sudan IV supersaturated in 38% 2-propanol) for 16 h at 4°C. A digital camera was used to capture images of the entire aortic tree. The total number of pixels covering the aorta area and the plaque lesions was measured using Adobe Photoshop CS3 (Adobe Systems Inc., San Jose, CA, USA). The percent (%) of the total surface area covered by the plaque in the aorta was then calculated.

2.2.3. Histochemistry. Small sections of the aorta were fixed with PLP for 16 h at 4°C. After fixation, samples were processed and embedded in paraffin. Serial sections from the aorta samples were obtained at a thickness of 4 μm. The sections were stained with H&E for morphometric analysis and with Masson's trichrome stain to identify collagen accumulation and smooth muscle cells (SMCs) in the plaque.

2.2.4. Immunohistochemistry. Macrophages and SMCs were quantitated in serial sections from the aorta samples using immunohistochemistry. The immunoperoxidase technique was employed and all slides were incubated in 0.3% H_2O_2 for 15 min to inhibit endogenous peroxidase activity and with Blocking One Histo solutions (Nacalai Tesque, Kyoto, Japan) for 10 min. Individual slides were incubated with one of the following: mouse anti-human CD68 monoclonal antibody (DAKO Japan, Tokyo, Japan, Cat. #M814), mouse anti-human α-smooth muscle actin (α-SMA) monoclonal antibody (DAKO Japan, Cat. #M0851), or mouse anti-human nonmuscle myosin heavy chain monoclonal antibody (SMemb; Yamasa, Tokyo, Japan, Cat. #7602) to detect macrophages, general SMCs, and synthetic SMCs, respectively. The slides were subsequently incubated with horseradish peroxidase- (HRP-) labeled goat anti-mouse immunoglobulin antibody (DAKO Japan, Cat. #K4001). The chromogen DAB was utilized to visualize staining and the slides were counterstained with hematoxylin thereafter. For immunohistochemical staining of rabbit macrophages, the slices were postfixed in 0.1 M phosphate buffer containing 4% paraformaldehyde for 30 min at 4°C. After washing by phosphate-buffered saline with 0.3% Toriton X-100 (PBS-T) 3 times in 5 min, the endogenous biotins were blocked by 0.3% H_2O_2 in PBS. The sections were rinsed 3 times for 10 min in PBS-T, incubated with 5% normal horse serum

in PBS-T for 1 hour at room temperature for blocking, and then incubated overnight with primary antibody, monoclonal mouse anti-rabbit macrophage (clone RAM11; diluted 1 : 50; DAKO, Glostrup, Denmark) in PBS-T at 4°C. After treatment of secondary antibody, the sections were incubated with ABC kit solutions (Vectastain, Vector Labs. Inc., Burlingame, CA) and then with the peroxidase substrate 3,3-diaminobenzidine (Wako, Osaka, Japan) for 10 min at room temperature for staining.

2.3. MRI and [^{18}F]FDG-PET

2.3.1. MRI. The monkeys were sedated by administering pentobarbital (30 mg/kg) intravenously into the inferior limbic vein through a plastic catheter. Aortas were imaged with a 3-Tesla MR scanner (Allegra; Siemens Medical, TX) using a 4-channel coil. Axial T2-weighted images were acquired with a turbo spin echo sequence (echo time, 15 ms; repetition time, 1500 ms; flip angle, 90°; section thickness, 3.0 mm; 24 slices; number of excitations, 8; echo train length, 7; field of view, 170–210 mm; data matrix, 384 × 384 pixels; matrix size = 0.4 × 0.4 × 3.0 mm or 0.5 × 0.5 × 3.0 mm). The MR imaging data were displayed using PMOD software (PMOD Technologies LLC, Zürich, Switzerland) for coregistration with arterial and blood-flow PET images.

2.3.2. [^{18}F]FDG-PET. The monkeys were fasted overnight and no significant differences were detected in the preprocedural blood glucose levels, which were less than 100 mg/dL in all monkeys. The monkeys were anesthetized by intramuscular injection of a solution of ketamine (10 mg/kg) and atropine (0.08 mg/kg), and the inferior limbic vein was catheterized. Each monkey was placed in a sitting position on a monkey chair for 3 h to recover from anesthesia. [^{18}F]FDG (37 MBq/kg) was injected into the vein through a plastic catheter, followed by a bolus injection of propofol (25 mg/kg) 30 min later and continuous infusion (10 mg/kg/h) until the end of the PET scan. Anesthetized monkeys were placed on the bed of a PET scanner for animals (microPET Focus-220, Siemens Preclinical Solution, Knoxville, TN, USA) and physiological parameters (electrocardiograph, heart rate, SpO_2, and body temperature) were regularly monitored throughout the PET scan. Emission data were acquired for 30 min at 90 min after injection of [^{18}F]FDG with gating ECG. After the emission scan, [^{18}F]FDG (15 MBq/kg) was reinjected to acquire a blood-flow image for identifying the location of the thoracic artery. The acquired emission data were reconstructed using a filtered back-projection algorithm with no attenuation and scatter corrections. For semiquantitative analysis, the regions of interests (ROIs) were manually drawn on the PET images at diastole. [^{18}F]FDG uptake in the aorta was evaluated using the target-to-background ratio (TBR), which is the ratio of radioactivity of the vessel wall to the lumen in the thoracic aorta [18].

2.4. Ex Vivo Macro- and Micro-ARG

2.4.1. Ex Vivo Macro-ARG. To further confirm the distribution of [^{18}F]FDG uptake in the aortas, ex vivo macro-ARG was conducted in the control and 7- and 12-month high-cholesterol diet groups ($N = 2$ in each group). The monkeys were given [^{18}F]FDG (37 MBq/kg) in the inferior limbic vein through a plastic catheter, followed by pentobarbital (30 mg/kg) 50 min after injection. The deeply anesthetized monkeys were euthanized by intracardiac perfusions of ice-cold 10 mM phosphate-buffered saline (pH 7.4) 60 min after injection of [^{18}F]FDG. The aortas were immediately dissected on ice, and several coronal sections of the aortas were sliced at a thickness of 20 μm using a cryostat and stored for histochemical and immunohistochemical analyses. The coronal sections were mounted on MAS-coated slides (Matsunami Glass, Osaka, Japan) and air-dried. The slides were placed in contact with an imaging plate (SR-2040, GE Healthcare, Tokyo, Japan) for 3 h to obtain the autoradiograms. The exposed imaging plates were measured using an image analyzer (FLA-7000IR; GE Healthcare). The data were quantified using a software ImageGage ver 4.0 (GE Healthcare). The sections were then stained with H&E. Simultaneously, the remainder of the whole aortas were dissected longitudinally and placed on black plastic plates with the lumen-side up. The aortas were fixed in PLP for 16 h at room temperature, rinsed with H_2O, and stained with Sudan IV solution for 16 h at 4°C. To investigate the localization of [^{18}F]FDG uptake in arterial wall in the representative animal model of atherosclerosis, ex vivo macro-ARG with [^{18}F]FDG was also performed in the WHHL and normal rabbits. [^{18}F]FDG at a dose of 37 MBq/kg was administered intravenously via the auricular vein under pentobarbital anesthesia. After injection of [^{18}F]FDG, animals were euthanized with an overdose of pentobarbital and perfused intracardiacally with ice-cold saline. The dissected arteries were cut at 20 μm thickness by using a cryostat. The slices were immediately contacted with an imaging plate (Fuji Film, Tokyo, Japan) for 2 hours, and it was scanned by a bioimaging analyzer. The image data were quantified with the radioactivity as an index of [^{18}F]FDG uptake was calculated from photo-stimulated luminescence (PSL) in area (mm^2) by scaling the injected dose of [^{18}F]FDG (MBq/kg). To obtain histological fusion images of macro-ARG, H&E staining was performed on the same slices after ARG.

2.4.2. Ex Vivo Micro-ARG. Ex vivo micro-ARG with [^{18}F]FDG was performed as described previously [14]. Briefly, under unexposed environmental conditions, several coronal sections of the aortas were sliced at a thickness of 4 μm using a cryostat and mounted on slides coated with a nuclear emulsion (NTB2; Kodak, NY) diluted 13 : 7 with distilled water. The slides were immediately frozen in dry ice and placed in exposure boxes that were maintained in dry ice for 6 h. Afterwards, the coronal sections were transferred to ethanol containing 5% v/v acetate at −70°C and 25°C for 1 min each. After a short wash in distilled water, the sections were immersed in Kodak D-19 developer for 5 min and fixed (Fuji Fix, Fuji Photo Film, Tokyo, Japan) for 15 min at room temperature. Finally, the sections were washed in distilled water for 10 min. After obtaining the images, the sections were used for immunohistochemistry analyses, as described above. Thereafter, the signals of [^{18}F]FDG grains

Table 1: Plasma lipids level in the monkeys after feeding of high-cholesterol diet.

Groups	Total-C (mg/dL)	HDL-C (mg/dL)	Free-C (mg/dL)	Triglyceride (mg/dL)
Control ($N = 8$)	149 ± 8	69.6 ± 5.7	34.3 ± 3.3	24.2 ± 4.0
7 M ($N = 8$)	426 ± 51*	36.9 ± 7.0*	84.3 ± 19.5*	7.3 ± 1.6*
12 M ($N = 6$)	292 ± 54	26.1 ± 4.9*	64.0 ± 11.5	85.2 ± 48.0
18 M ($N = 4$)	330 ± 78	43.8 ± 16.8	73.9 ± 13.5*	104.4 ± 45.5
24 M ($N = 3$)	304 ± 13*	28.3 ± 5.5*	70.0 ± 3.4*	57.9 ± 27.1

Data are presented as mean and SEM. * $p < 0.05$ versus control by ANOVA with Bonferroni's correction.

associated with macrophages or SMCs were analyzed in the neointima or media. Total neointimal and medial areas were measured and the areas of [^{18}F]FDG grain colocalization with macrophages or SMCs were measured against five randomly selected 1600 × 1000 μm^2 fields. Finally, [^{18}F]FDG grains colocalized with these cells were estimated in the neointima and media. All measurements were performed using Photoshop CS3.

2.5. Statistical Analyses. The data are presented as means and standard error of the mean. One-way analysis of variance (ANOVA) was used to evaluate differences in the biochemical parameters between the 5 experimental groups, as well as differences in grain-positive areas between the early and late groups. When statistically significant effects were found, intergroup differences were compared using Student's t-test with Bonferroni correction. Statistical significance was set at $p < 0.05$.

3. Results

3.1. Biochemical Parameters and Histological Analyses

3.1.1. Biological Parameters. Total-C and free-C levels were higher in high-cholesterol-fed monkeys than in control monkeys (Table 1). Conversely, HDL-C levels were lower in high-cholesterol-fed monkeys than in the controls. Cholesterol was mostly packaged in LDL, which was confirmed by HPLC analysis (data not shown). There were no significant differences in other biochemical parameters among the groups.

3.1.2. Analysis of Atherosclerotic Lesions of Whole Aorta. No atherosclerotic plaques were found in the control monkeys. On the other hand, plaque surface area in aortic trees increased as the duration of high-cholesterol diet increased from 7 to 24 months (Figure 1).

3.1.3. Histochemistry and Immunohistochemistry. H&E staining of control aortas revealed an intact endothelial cell layer and SMC layer. The medial region was composed of SMCs and collagen depositions. There were no macrophages in the control aortic wall. In contrast, H&E staining of aortas dissected from monkeys fed the high-cholesterol diet for 7 months revealed a well-formed neointima with possible droplets of lipid accumulation. Neointimal SMCs were highly positive for SMemb, but collagen depositions were scarce. Macrophages were colocalized with the putative lipid droplets. The neointimal thickness gradually increased as the duration of high-cholesterol diet feeding increased up to 24 months. Trichrome staining revealed massive collagen depositions in the neointima at 12, 18, and 24 months of high-cholesterol diet. Macrophages and SMemb-positive SMCs were also more prominent in the aortas of monkeys fed the high-cholesterol diet for 24 months (Figure 2). Apparently, we observed unstable plaques in this simian model which were similar to those in humans.

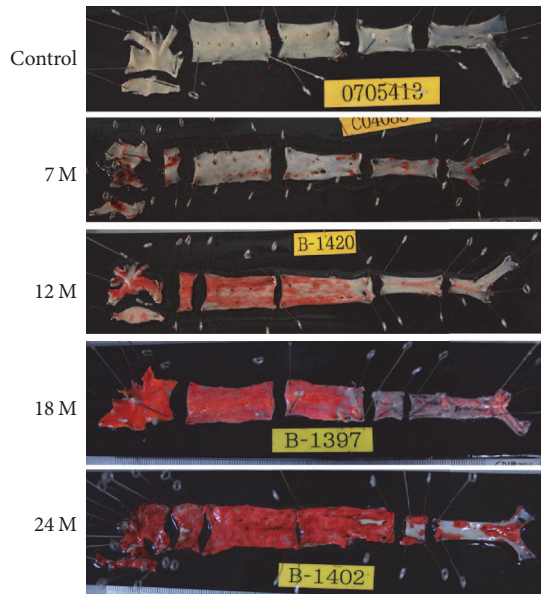

Figure 1: Plaque formation in aortic trees. Sudan IV staining shows the extent of lipid-containing plaques (red/orange stains) in aortic trees of monkeys fed control or high-cholesterol diet for 7, 12, 18, and 24 months.

3.2. In Vivo MRI-PET Imaging. High [^{18}F]FDG uptake was observed in the thoracic aortas and the aortic arches, which were the most common sites of arteriosclerotic lesion in high-cholesterol-fed and control monkeys (Figure 3). A tendency of increase of thoracic arterial [^{18}F]FDG uptake was observed in monkeys with the high-cholesterol diet for 18 and 24 months (0.62±0.19 and 0.57±0.19 in TBR, resp.) as compared

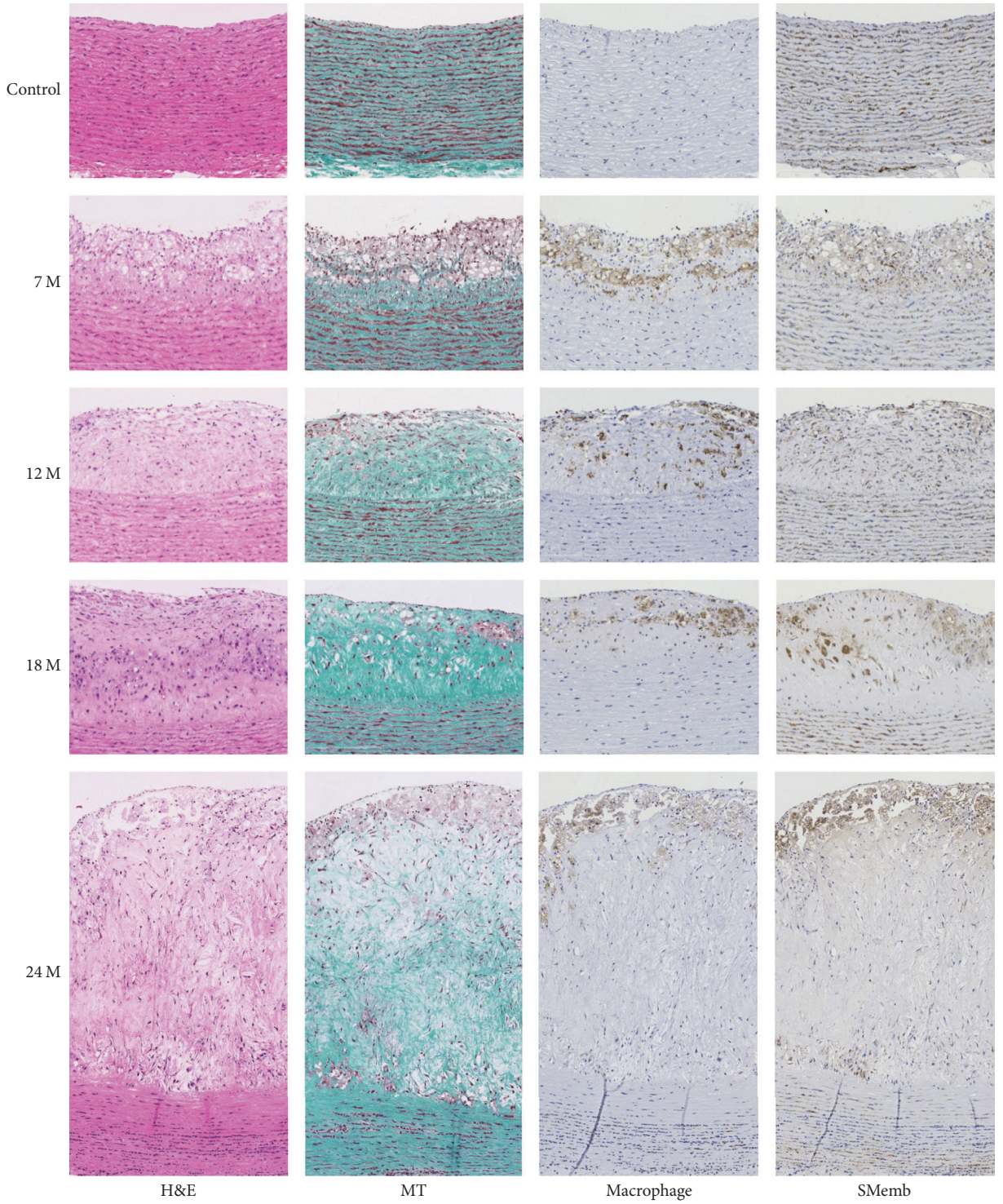

Figure 2: Histochemical and immunohistochemical analyses of plaques. Masson's trichrome stain (MT), anti-macrophage, and anti-SMemb-positive SMC staining of aorta tissue from control and high-cholesterol diet fed monkeys are displayed.

with that in the controls (0.21 ± 0.03 in TBR), while no increase in [^{18}F]FDG uptake was observed in monkeys for 7 and 12 months at all (0.11 ± 0.09 and 0.22 ± 0.15 in TBR, resp.). Therefore, the monkeys fed the high-cholesterol diet for 7 to 12 months and 18 to 24 months were defined as the "Early group" and "Late group," respectively.

3.3. Ex Vivo Macro- and Micro-ARG

3.3.1. Ex Vivo Macro-ARG. After PET/MRI experiment, since we observed increases in aortic wall thickness and in accumulation of [^{18}F]FDG in arterial sections of high-cholesterol-fed monkeys at 7 and 12 months as compared with the control

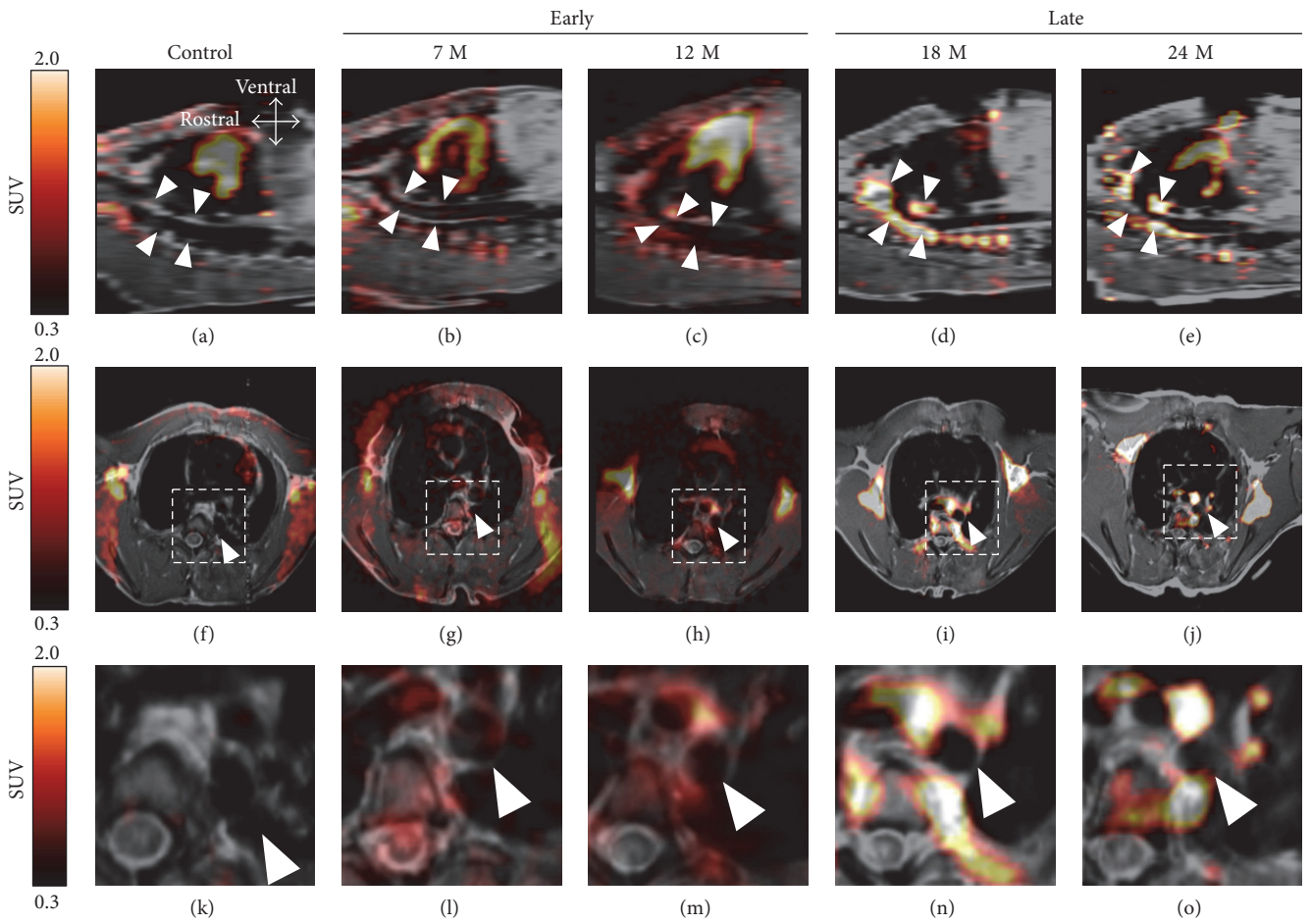

Figure 3: PET images of [^{18}F]FDG uptake in the simian model of arteriosclerosis. Sagittal (a–e) and coronal (f–j) images are shown. Corresponding sections (k–o) are from the dashed box regions of (f–j), respectively. Images are from control animals (a, f, k), animals fed a high-cholesterol diet for 7 (b, g, l) and 12 (c, h, m) months as the "Early" phase and for 18 (d, i, n) and 24 months (e, j, o) as the "Late" phase. White arrowheads indicate the thoracic aorta.

monkeys (Figure 4), we further performed ex vivo macro-ARG to identify the localization of changes in [^{18}F]FDG uptake in arterial section. Merging of H&E staining and [^{18}F]FDG signals clearly indicated colocalization in the thickened aortic walls of high-cholesterol-fed monkeys at 7 and 12 months (Figure 4). In control monkeys, very thin endothelial (intima) and smooth muscle cell layers (media) were distinguishable using high magnification images. In contrast, both the intima and media were thickened in high-cholesterol-fed monkeys at 7 and 12 months. [^{18}F]FDG signals were mostly localized in both the media and intima (Figure 4). In the case of WHHL rabbits, [^{18}F]FDG uptakes in the aorta sections were also observed extensively in both the neointima and media, which were characterized by the presence of invading macrophages and vascular SMCs (Figure 5).

3.3.2. Ex Vivo Micro-ARG. Ex vivo micro-ARG clearly indicated that the majority of [^{18}F]FDG grains were observed in the media and were largely absent in the neointima (Figure 6(a)). Ex vivo micro-ARG followed by anti-CD68 staining demonstrated that macrophages in the neointima were not colocalized with high-density [^{18}F]FDG grains (Figure 6(b)). Furthermore, no macrophages were observed in the media (data not shown). Ex vivo micro-ARG followed by anti-SMemb or anti-SMA staining demonstrated that focal accumulation of [^{18}F]FDG grains was mainly colocalized with SMCs (Figure 6(c)). The majority of the [^{18}F]FDG grains were observed in the media, especially in the SMC layers (Figure 6(d)). Quantitative analysis in the different stage during lesion progression clearly demonstrated that [^{18}F]FDG primarily accumulated locally into cells in the medial layer in both the "Early" and "Late groups" (Figure 6(e)). Although macrophages in the neointima tended to take up more [^{18}F]FDG than SMCs in the "Late group," the difference was not statistically significant, and the accumulation by macrophage itself did not significantly contribute to total [^{18}F]FDG uptake in the locus (Figures 6(e) and 6(f)).

4. Discussion

The main results of our study using ex vivo macro- and micro-autoradiography with [^{18}F]FDG in our simian model of

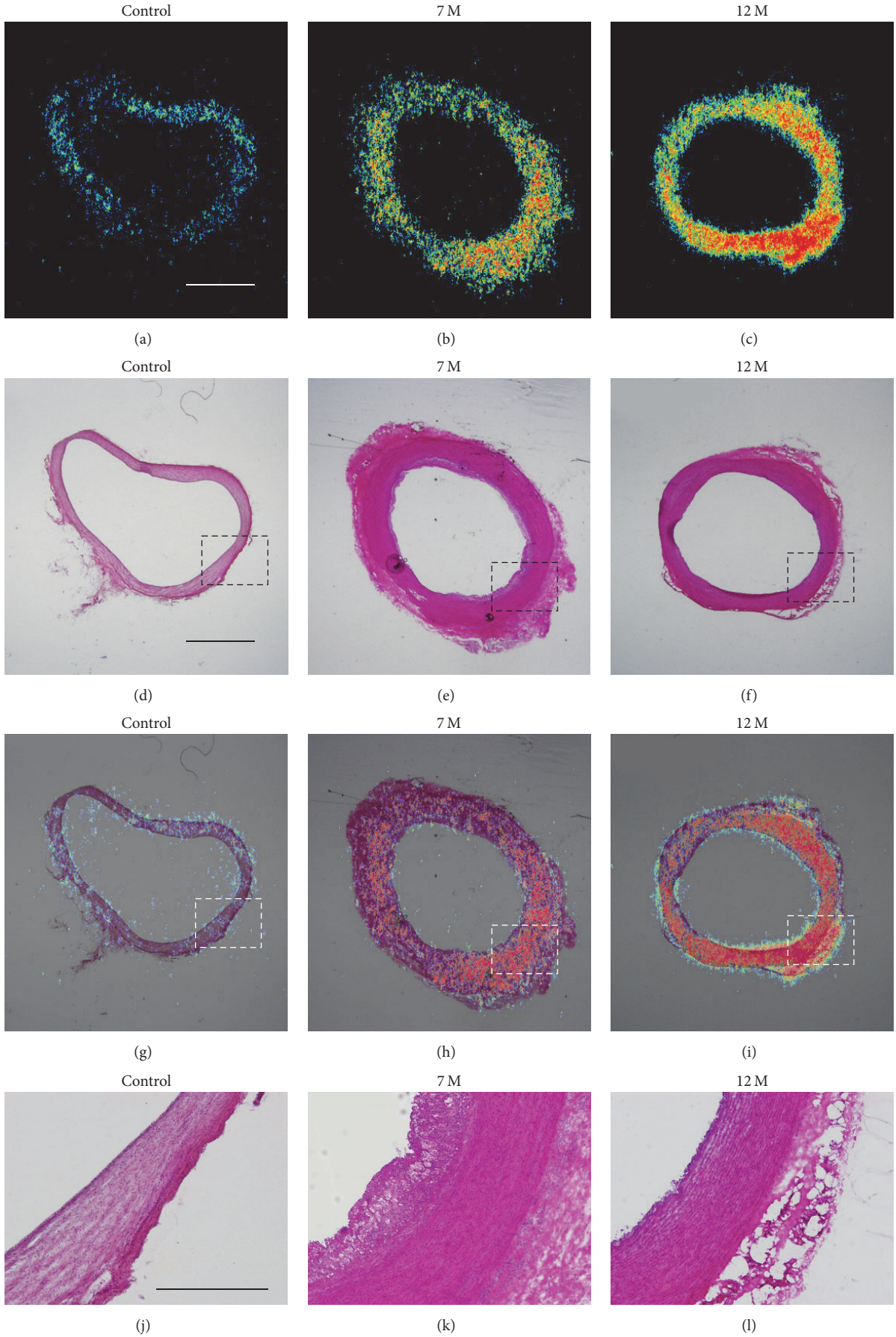

Figure 4: Continued.

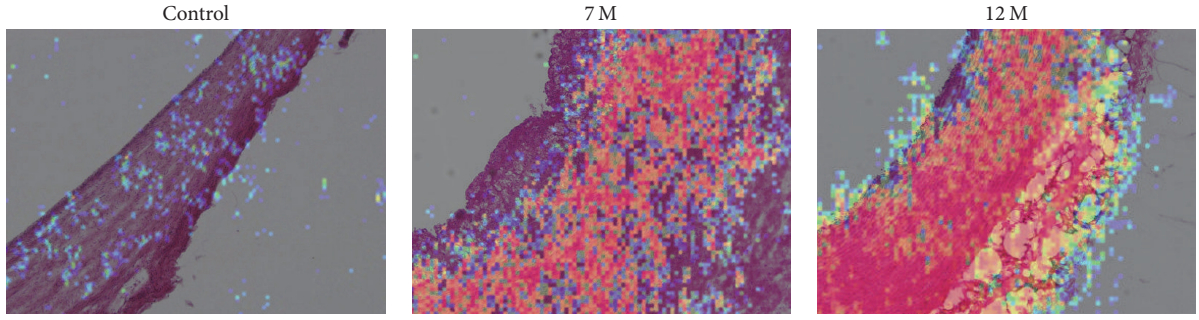

Figure 4: Localization of [^{18}F]FDG uptake in coronal sections of the thoracic aorta. Macro-autoradiograms with [^{18}F]FDG (a–c), H&E staining (d–f), and merged images (g–i). Tissues from control animals (a, d, g) and animals fed a high-cholesterol diet for 7 (b, e, h) and 12 months (c, f, i). (j–o) are the corresponding sections from dashed box regions of (d–i), respectively. (a–i), bar = 2 mm; (j–o), bar = 300 μm.

atherosclerosis were as follows: (1) [^{18}F]FDG was highly accumulated in the vascular media as well as the vulnerable plaque in the intima; (2) high uptake of [^{18}F]FDG in the media, which was not observed in the control animals, was identified not only in the infiltrated macrophages in atherosclerotic lesions but also in the SMCs. Though numerous studies have indicated that high [^{18}F]FDG uptake measured by PET is closely related to cell numbers and/or activation of infiltrated macrophages accumulated in atherosclerotic vulnerable plaques [13, 14], our study has revealed that [^{18}F]FDG uptake was localized in both the intima and media including the SMCs by accurate quantification of atherosclerotic lesions at tissue and cellular levels.

Atherosclerotic plaques are comprised of several different cell types, of which macrophages and SMCs are the predominant populations. While SMCs produce extracellular matrices to stabilize plaques, macrophages uptake modified LDL, especially oxidized LDL *via* scavenger receptors, to clear excessive lipid accumulation. In this process, both macrophages and SMCs protect atherosclerotic vessels in the early stages similar to those in wound healing [17]. However, uptake of oxidized LDL by macrophages causes intracellular accumulation of cholesterol and precipitates their transformation to foam cells. Foam cells produce several proteinases, which degrade extracellular matrices, thereby increasing the fragility of plaques [19]. Moreover, foam cells express tissue factors on their membrane, which initiate the extrinsic blood coagulation cascade. Blood clots are rapidly formed when foam cells penetrate the endothelial cell layer and come into contact with the blood stream, ultimately leading to arterial occlusion [19]. Thus, excessive activation of macrophages in plaques is ultimately destructive. Therefore, it becomes a more important matter to detect macrophages (and their activity) in atherosclerotic plaques.

Ogawa et al. recently reported that [^{18}F]FDG-PET signals in atherosclerotic plaques were highly dependent on the number of infiltrated macrophages in the thoracic aorta in WHHL with myocardial infarction [13, 20]. They also investigated in vitro [^{18}F]FDG uptake using isolated SMCs from C57Bl/6 male mice and macrophages from female ddY mice to elucidate the primary cell types that take up [^{18}F]FDG in hypercholesterolemia. Their conclusion was that only early-stage plaque-infiltrating macrophages, but not SMCs of the aortic wall, are visualized by [^{18}F]FDG [21]. However, SMCs are also transformed into foam cells when cultured with modified LDL [22], and expression levels and/or patterns of scavenger receptors in macrophages and SMCs are different between C57Bl/6 and ddY mice [23].

Our simian atherosclerosis model demonstrated that well-formed atherosclerotic plaques developed from the ascending aorta to the descending aorta. Histological and immunohistological analyses revealed that plaques in this simian model contained early-stage macrophages and SMCs and that these cells were accompanied with collagen depositions and lipid-laden necrotic cores in the late stages. These patterns are similar to those observed in other animal models, although macrophage infiltration into plaques is more evident in the WHHL rabbit model [3–5, 24].

[^{18}F]FDG uptake was more intense in the aortic wall at later time points, suggesting that [^{18}F]FDG accumulation is correlated to the severity of atherosclerosis. We have also confirmed that [^{18}F]FDG accumulation in the WHHL rabbit model is observed in the neointima using ex vivo macro-ARG. However, in the simian model, the majority of [^{18}F]FDG was absorbed by SMCs in the media and not by macrophages or SMCs in the neointima, as confirmed by ex vivo macro-ARG. These results indicate that the localization of [^{18}F]FDG uptake is dependent on species and disease progression. Considering these factors, the translation of results of animal studies to humans must be performed with extreme caution, and intensive studies using more humanized models are required.

In clinical PET studies of atherosclerotic patients, inconsistent results were reported in relation to the correlation between [^{18}F]FDG signal and macrophage infiltration detected using immunohistochemical staining of biopsy samples [13, 15]. [^{18}F]FDG-PET is quite useful for quantitative assessment of lesion progression in atherosclerosis. However, it is difficult to distinguish [^{18}F]FDG uptake in the vulnerable plaques from that in vascular component or surrounding

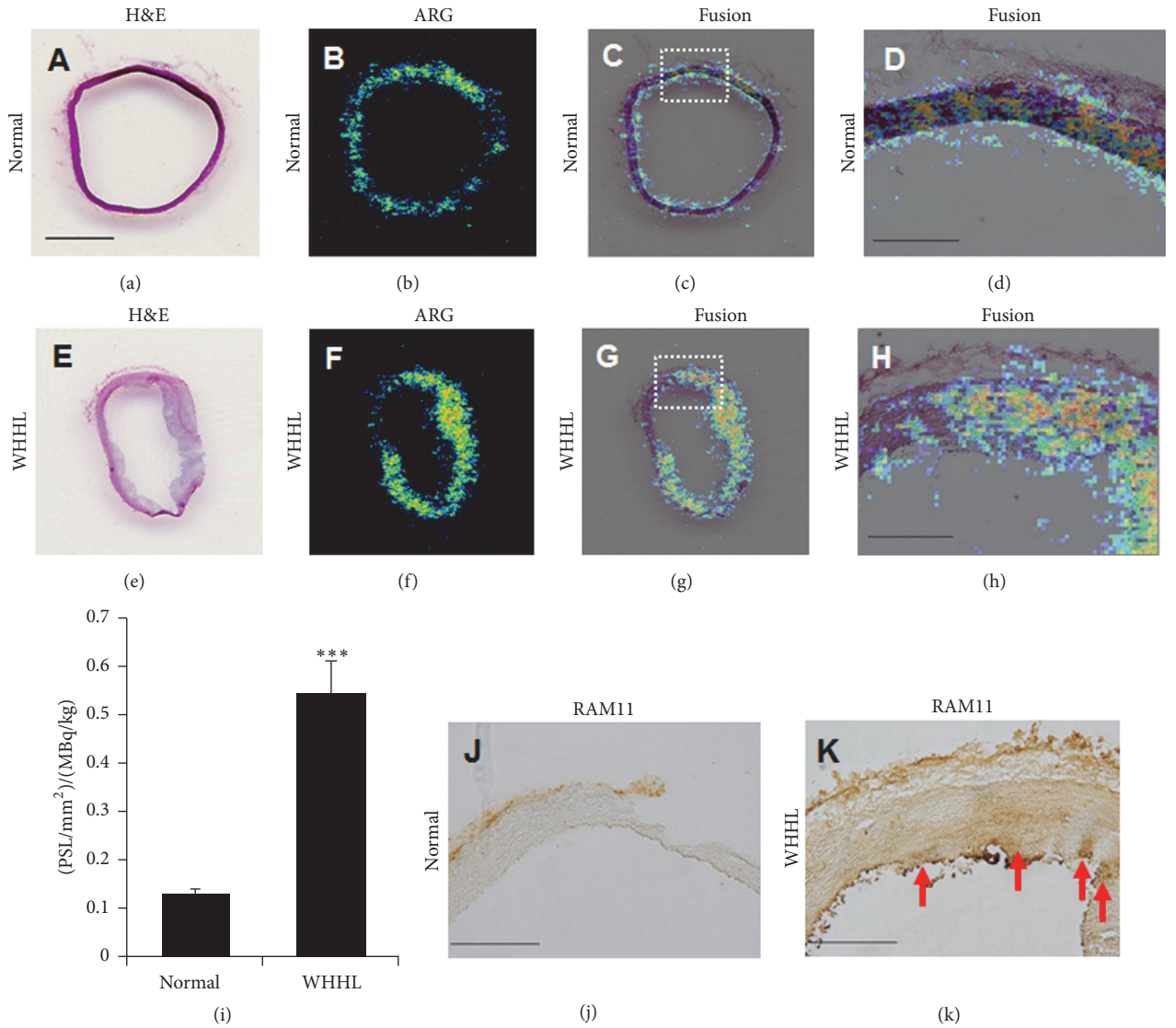

FIGURE 5: Histological analysis of thoracic aorta of rabbit model of atherosclerosis. The arterial slices in the normal and WHHL rabbits at age of 6 months ((a–d), normal; (e–h), WHHL). H&E staining (a and e) and ex vivo macro-autoradiograms with [^{18}F]FDG (b and f) and fusion images (c and g). (d and h) are the corresponding sections from dashed line of (c and g), respectively. Arterial [^{18}F]FDG uptake values which were quantified with serial 2 slices from each animal were compared between the normal and WHHL rabbits (i). $^{***}P < 0.001$ versus control. The data represent mean and s.e.m. ($n = 2 \times 2$ slices). Immunohistochemical staining of macrophage by RAM11, anti-rabbit macrophage, in the arterial vessel ((j), normal; (k), WHHL). Red arrows indicate RAM-positive cells in the aorta of WHHL rabbit. The slices at 20 μm thickness. (a–c), (e–g), bar = 1 mm; (d), (j), and (k), bar = 300 μm.

normal tissues in PET imaging, which may be due to its low spatial resolution at a range of a few millimeter and partial volume effect as specific problems of the imaging scanner [25]. In addition, our PET study has limited quantitative assessment because of the lack of attenuation and scatter corrections. In our preliminary experiments, we performed transmission scan using a ^{68}Ge-^{68}Ga point source before [^{18}F]FDG injection under anesthesia and reconstructed PET images according to the conventional data procedure. However, unexpectedly, [^{18}F]FDG uptake showed low TBR with low arterial and high intravascular radioactivities, probably caused by low blood clearance of [^{18}F]FDG under anesthetic condition. To improve the TBR in the atherosclerotic lesion, we modified the scan protocol, in particular, no anesthesia during [^{18}F]FDG uptake period until the PET scanning to keep the animal under physiological state, whereas no preinjection transmission was available in this procedure. Since ^{68}Ge-^{68}Ga-based radioactivity was low in PET scanner used in this study, which was insufficient for postinjection transmission scan, it was very difficult to use as accurate attenuation and scatter corrections [26]. To overcome the limitation, CT-based reconstruction using CT or hybrid PET/CT system will be useful to get reliable attenuation and scatter corrections with accurate coregistration with PET

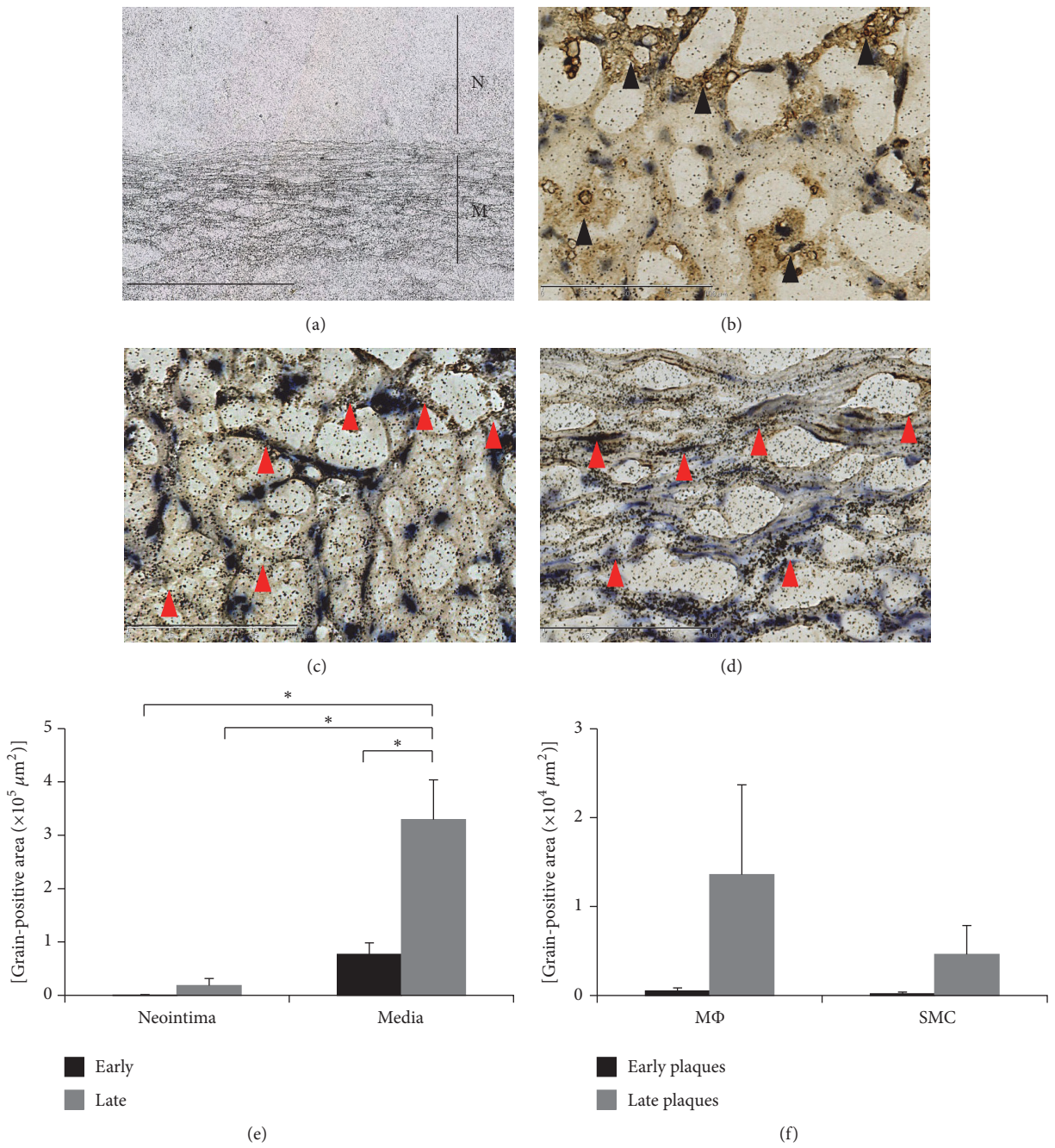

FIGURE 6: Micro-autoradiography. Lower magnification ex vivo micro-ARG image of [^{18}F]FDG grains in neointima and media from monkeys fed a high-cholesterol diet for 24 months (bar = 400 μm) (N, neointima; M, media) (a). Higher magnification ex vivo micro-ARG image of [^{18}F]FDG grains in neointima (bar = 100 μm) (b). [^{18}F]FDG grains and SMCs in neointima: red arrowheads indicate SMCs (bar = 400 μm) (c). [^{18}F]FDG grains and SMCs in media: red arrowheads indicate SMCs (bar = 400 μm) (d). Measurement of [^{18}F]FDG grain-positive areas in neointima and media ($^{*}p < 0.05$) (e). Measurement of [^{18}F]FDG grain-positive area in macrophages (MΦ) and SMCs in neointima (f).

image. Our results also indicate the limitation of in vivo [^{18}F]FDG-PET images for identification of atherosclerotic lesions, but in the present study, we used a combined analysis of ex vivo micro-ARG with immunohistochemical staining to assess the precise cellular origin of [^{18}F]FDG signals and demonstrated that its predominant localization is in aortic SMCs of atherosclerotic vessels and in infiltrated macrophages. Therefore, it is likely that the inconsistency observed in the clinical studies is due to the poor spatial resolution of PET, which can lead to inaccurate evaluations in imaging analysis [25].

Oxidized LDL is known to stimulate aortic SMC proliferation [27]. Medial SMCs activated by modified LDL may take up more [^{18}F]FDG than macrophages, and the intensity

of medial SMC [^{18}F]FDG signals is correlated to the extent of plaque formation in the aorta. Taken together, these results indicate that the intensity of [^{18}F]FDG signals is useful for identifying the pathology of sclerotic arteries covered with plaques in the simian model of atherosclerosis.

5. Conclusion

We developed a simian atherosclerosis model by feeding the high-cholesterol diet and performed in vivo PET, ex vivo macro- and micro- ARG. Progressively increased [^{18}F]FDG uptake in the aortic wall was observed in high-cholesterol diet-treated monkeys by PET. Combined analysis of ex vivo ARG with immunohistochemistry revealed that high [^{18}F]FDG uptake observed in the media was derived not only from the infiltrated macrophages in atherosclerotic plaques but also from the smooth muscle cells (SMCs) of the aortic wall in atherosclerotic lesions.

Competing Interests

The authors declare that they have no conflict of interests.

Authors' Contributions

Takayuki Iwaki, Hiroshi Mizuma, and Kazuya Hokamura are equally contributing authors.

Acknowledgments

The authors thank Ms. Ayami Hori and Dr. Kenichi Kawano for performing the histological and pathohistological analyses, Mr. Masahiro Ohno for technical assistance in the imaging study, and Dr. Tatsuo Tanimoto and Dr. Nobuya Kurikawa (Daiichi-Sankyo Co. Ltd.) for measuring plasma lipid levels and evaluating the PET images and for providing editorial assistance. This work was supported in part by the Japan Society for the Promotion of Science (JSPS) KAKENHI 20890093 and 22790247 (to Takayuki Iwaki), the Uehara Memorial Foundation (to Takayuki Iwaki), and the Molecular Imaging Research Program from the Ministry of Education, Culture, Sports, Science, and Technology of the Japanese Government (05009013). They thank Dr. Hiroyuki Takamatsu (Hamamatsu Pharma Research, Inc.) for performing welfare and management in monkeys.

References

[1] R. Ross, "The pathogenesis of atherosclerosis: a perspective for the 1990s," *Nature*, vol. 362, no. 6423, pp. 801–809, 1993.

[2] S. Ishibashi, M. S. Brown, J. L. Goldstein, R. D. Gerard, R. E. Hammer, and J. Herz, "Hypercholesterolemia in low density lipoprotein receptor knockout mice and its reversal by adenovirus-mediated gene delivery," *Journal of Clinical Investigation*, vol. 92, no. 2, pp. 883–893, 1993.

[3] L. Powell-Braxton, M. Véniant, R. D. Latvala et al., "A mouse model of human familial hypercholesterolemia: markedly elevated low density lipoprotein cholesterol levels and severe atherosclerosis on a low-fat chow diet," *Nature Medicine*, vol. 4, no. 8, pp. 934–938, 1998.

[4] A. S. Plump, J. D. Smith, T. Hayek et al., "Severe hypercholesterolemia and atherosclerosis in apolipoprotein E-deficient mice created by homologous recombination in ES cells," *Cell*, vol. 71, no. 2, pp. 343–353, 1992.

[5] Y. Watanabe, "Serial inbreeding of rabbits with hereditary hyperlipidemia (WHHL-rabbit). Incidence and development of atherosclerosis and xanthoma," *Atherosclerosis*, vol. 36, no. 2, pp. 261–268, 1980.

[6] A. D. Attie, R. C. Pittman, Y. Watanabe, and D. Steinberg, "Low density lipoprotein receptor deficiency in cultured hepatocytes of the WHHL rabbit. Further evidence of two pathways for catabolism of exogenous proteins," *Journal of Biological Chemistry*, vol. 256, no. 19, pp. 9789–9792, 1981.

[7] G. Vilahur, T. Padro, and L. Badimon, "Atherosclerosis and thrombosis: insights from large animal models," *Journal of Biomedicine and Biotechnology*, vol. 2011, Article ID 907575, 12 pages, 2011.

[8] M. R. Malinow and C. A. Maruffo, "Aortic atherosclerosis in free-ranging howler monkeys (Alouattacaraya)," *Nature*, vol. 206, no. 4987, pp. 948–949, 1965.

[9] M. Magnoni, E. Ammirati, and P. G. Camici, "Non-invasive molecular imaging of vulnerable atherosclerotic plaques," *Journal of Cardiology*, vol. 65, no. 4, pp. 261–269, 2015.

[10] V. Sandfort, J. A. C. Lima, and D. A. Bluemke, "Noninvasive imaging of atherosclerotic plaque progression: status of coronary computed tomography angiography," *Circulation: Cardiovascular Imaging*, vol. 8, no. 7, Article ID e003316, 2015.

[11] J. M. Tarkin, M. R. Dweck, N. R. Evans et al., "Imaging atherosclerosis," *Circulation Research*, vol. 118, no. 4, pp. 750–769, 2016.

[12] J. M. U. Silvola, A. Saraste, I. Laitinen et al., "Effects of age, diet, and type 2 diabetes on the development and FDG uptake of atherosclerotic plaques," *JACC: Cardiovascular Imaging*, vol. 4, no. 12, pp. 1294–1301, 2011.

[13] M. Ogawa, Y. Magata, T. Kato et al., "Application of 18F-FDG PET for monitoring the therapeutic effect of antiinflammatory drugs on stabilization of vulnerable atherosclerotic plaques," *Journal of Nuclear Medicine*, vol. 47, no. 11, pp. 1845–1850, 2006.

[14] A. Tawakol, R. Q. Migrino, U. Hoffmann et al., "Noninvasive in vivo measurement of vascular inflammation with F-18 fluorodeoxyglucose positron emission tomography," *Journal of Nuclear Cardiology*, vol. 12, no. 3, pp. 294–301, 2005.

[15] K. S. Myers, J. H. F. Rudd, E. P. Hailman et al., "Correlation between arterial FDG uptake and biomarkers in peripheral artery disease," *JACC: Cardiovascular Imaging*, vol. 5, no. 1, pp. 38–45, 2012.

[16] K. Shelton, T. Clarkson, and J. Kaplan, "Nonhuman primate models of atherosclerosis," in *Nonhuman Primates in Biomedical Research*, chapter 8, pp. 385–411, Elsevier, 2nd edition, 2012.

[17] M. Yamato, Y. Kataoka, H. Mizuma, Y. Wada, and Y. Watanabe, "PET and macro- and microautoradiographic studies combined with immunohistochemistry for monitoring rat intestinal ulceration and healing processes," *Journal of Nuclear Medicine*, vol. 50, no. 2, pp. 266–273, 2009.

[18] A. Tawakol, R. Q. Migrino, G. G. Bashian et al., "In vivo 18F-fluorodeoxyglucose positron emission tomography imaging provides a noninvasive measure of carotid plaque inflammation in patients," *Journal of the American College of Cardiology*, vol. 48, no. 9, pp. 1818–1824, 2006.

[19] P. Libby, P. M. Ridker, and G. K. Hansson, "Progress and challenges in translating the biology of atherosclerosis," *Nature*, vol. 473, no. 7347, pp. 317–325, 2011.

[20] M. Ogawa, S. Ishino, T. Mukai et al., " ^{18}F-FDG accumulation in atherosclerotic plaques: immunohistochemical and PET imaging study," *Journal of Nuclear Medicine*, vol. 45, no. 7, pp. 1245–1250, 2004.

[21] M. Ogawa, S. Nakamura, Y. Saito, M. Kosugi, and Y. Magata, "What can be seen by ^{18}F-FDG PET in atherosclerosis imaging? The effect of foam cell formation on ^{18}F-FDG uptake to macrophages in vitro," *Journal of Nuclear Medicine*, vol. 53, no. 1, pp. 55–58, 2012.

[22] R. E. Pitas, A. Friera, J. McGuire, and S. Dejager, "Further characterization of the acetyl LDL (scavenger) receptor expressed by rabbit smooth muscle cells and fibroblasts," *Arteriosclerosis, Thrombosis, and Vascular Biology*, vol. 12, no. 11, pp. 1235–1244, 1992.

[23] Y. Ikeda, A. Murakami, and H. Ohigashi, "Strain differences regarding susceptibility to ursolic acid-induced interleukin-1β release in murine macrophages," *Life Sciences*, vol. 83, no. 1-2, pp. 43–49, 2008.

[24] J. A. Piedrahita, S. H. Zhang, J. R. Hagaman, P. M. Oliver, and N. Maeda, "Generation of mice carrying a mutant apolipoprotein E gene inactivated by gene targeting in embryonic stem cells," *Proceedings of the National Academy of Sciences of the United States of America*, vol. 89, no. 10, pp. 4471–4475, 1992.

[25] D. Izquierdo-Garcia, J. R. Davies, M. J. Graves et al., "Comparison of methods for magnetic resonance-guided [18-f] fluorodeoxyglucose positron emission tomography in human carotid arteries: reproducibility, partial volume correction, and correlation between methods," *Stroke*, vol. 40, no. 1, pp. 86–93, 2009.

[26] W. Lehnert, S. R. Meikle, S. Siegel, D. Newport, R. B. Banati, and A. B. Rosenfeld, "Evaluation of transmission methodology and attenuation correction for the microPET Focus 220 animal scanner," *Physics in Medicine and Biology*, vol. 51, no. 16, pp. 4003–4016, 2006.

[27] S. Chatterjee and N. Ghosh, "Oxidized low density lipoprotein stimulates aortic smooth muscle cell proliferation," *Glycobiology*, vol. 6, no. 3, pp. 303–311, 1996.